Ultramicroscopy 253 (2023) 113772

Contents lists available at ScienceDirect

Ultramicroscopy

journal homepage: www.elsevier.com/locate/ultramic

# Quantitative comparison of excitation modes of tuning forks for shear force in probe microscopy

V.V. Tkachuk *, J.P. Korterik, H.L. Offerhaus

*Department of Science and Technology, Optical Sciences Group, University of Twente, P.O. Box 217, 7500 AE Enschede, The Netherlands*

ARTICLE INFO

*Keywords:*
SNOM
NSOM
Tuning fork
Shear force

ABSTRACT

This article provides a careful comparison between the electric and mechanical excitation of a tuning fork for shear force feedback in scanning probe microscopy, an analysis not found in present literature. A setup is designed and demonstrated for robust signal and noise measurements at comparable levels of physical movement of the probe. Two different signal amplification methods, combined with two excitation ways provide three possible configurations. For each method a quantitative analysis, supported by analytical elaboration and numerical simulations, is provided. Finally, it is shown that in practical circumstances electric excitation followed by detection with a transimpedance amplifier provides the best result.

## 1. Introduction and motivation

In any kind of scanning probe microscopy, the tip-sample interaction plays an important role in the quality the of measurements and longevity of the tip [1]. When using fiber tips in Near-field scanning optical microscopy (NSOM), a quartz tuning fork can be added near the fiber tip to provide a feedback signal to control the sample-tip height. The distance between the apex of the tip and the sample has to be kept constant at very close proximity, and the topology of the sample has to be followed with fine precision to avoid crashing [2]. NSOM tips are fragile compared to their cantilevered counterparts used in atomic force microscopy [3,4]. Also, tunneling feedback is usually not an option due to the fact that samples cannot be covered with a conductive layer without altering the optical properties. When using a tip scanner, as it is convenient to fix the sample to an optical in-coupling stage, force feedback cannot be accomplished by optical means (interferometric or shadow pattern), leaving only mechanical interaction suitable [5–7]. Somewhat surprisingly, the authors did not find a published systematic optimization of signal to noise ratios of tuning fork behavior in shear force feedback applications, despite nearly three decades since the introduction of this technique.

### 1.1. Tuning forks

Karraï et al. first attached commercially available tuning forks close to the fiber tip to obtain a signal for tip-sample distance control [8]. When excited near resonance at close proximity to the sample surface, the amplitude of the tip dampens due to shear force interaction [9,10]. The damping can be detected and this type of detection is conducive to optical scanning probe microscopy because it does not produce disturbances to the optical experiments other than the introduction of the tip itself. Resonant vibration of the apex of a fiber tip can be obtained by attaching the fiber to a (commercially available) quartz tuning fork (Fig. 1).

Two mechanisms can be employed to induce vibrations in the tip [11,12] (Fig. 3). The first is to mechanically excite vibration in the tuning fork by attaching the side of the base to a dither (shaker) piezo [13], driven with a signal close to the tuning fork's resonant frequency. In this configuration, the base of the tuning fork is rigidly attached to the piezo-actuator, and both prongs are initially driven to oscillate in the same direction (the symmetric or common mode) [14]. However, due to the design, the tuning fork assumes the mode in which the prongs move relative to each other (the asymmetric or differential mode). The latter usually has a resonance frequency in the range of 32–34 kHz, while the former has no resonance around 26–28 kHz (Fig. 2A, B). The electrodes on the piezo crystal are arranged in such a way that they collect the induced surface charges due to the oscillation in the differential mode and reject the common mode [11,15,16]. The drive (common mode) and the detection (differential mode) circuits are thus decoupled and the signal produced by the tuning fork electrodes is large enough for detection and is practically free from an excitation offset. The efficiency of the vibration transfer to the tuning fork and the mounting of the piezo determine the shape of the transfer characteristic which displays resonance features of all parts of the system. This results in multiple local resonances alongside the dominant peak in the amplitude and phase transfer characteristics (Fig. 6, red curves).

* Corresponding author.
*E-mail address:* v.tkachuk@utwente.nl (V.V. Tkachuk).

https://doi.org/10.1016/j.ultramic.2023.113772
Received 10 June 2022; Received in revised form 7 February 2023; Accepted 30 May 2023
Available online 5 June 2023

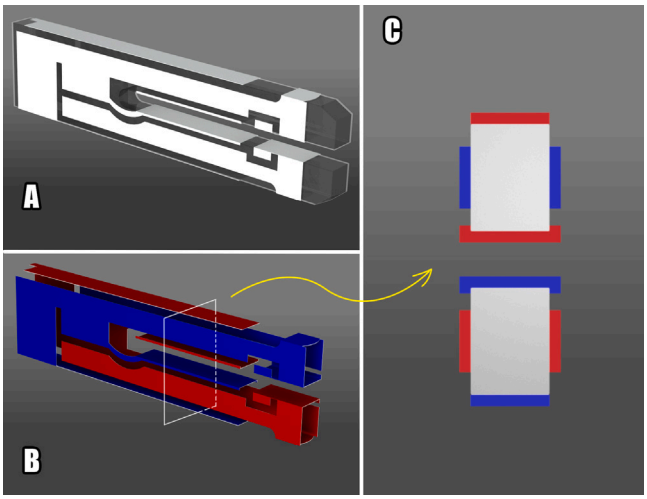


**Fig. 1.** Computer graphics image of a typical 32.768 kHz tuning fork. The leads, referred to as "1" in the overview picture (Fig. 4), are soldered to the red and blue contacts. A — Overview, the connection leads and enclosure are omitted. B — Layout of the electric contacts. C — Cross-section of the electrodes at the marked area in (B) (thickness exaggerated for better visibility).

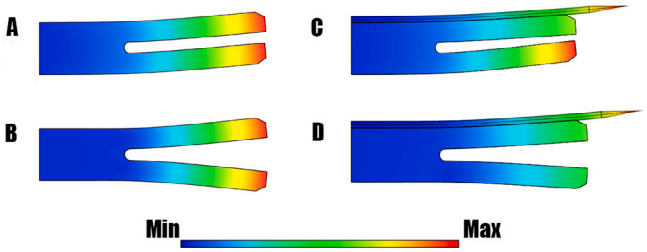


**Fig. 2.** The shapes representing the results of finite element modeling of tuning fork's natural resonant frequencies (the deformations are exaggerated). (A, C) common mode (28 kHz), (B, D) differential mode (32 kHz). The color represents their modulus of absolute deflection. A, B - without a fiber, C, D - with a fiber attached.

The second excitation mechanism is to apply an alternating voltage to the electrodes of the tuning fork. Due to the layout of the electrodes, only the differential mode oscillation will be excited efficiently [17] (Fig. 2B, D). The oscillation of the tuning fork induces a measurable signal current. In this manner, the vibration can be both excited and detected electronically. Due to the capacitance of the tuning fork (2 pF), however, there is a current offset independent of the mechanical motion [16].

Since the NSOM tips are fragile, the tip-sample interaction forces should be kept low and the amplitude of the oscillation of the tip should be kept low compared to the tip aperture (ca. 20 nm). This means that the signal across the tuning fork leads will be kept small, and hence the signal-to-noise ratio (SNR) of the detection system limits the resolution, the accuracy and the quality of the near-field measurements. In our case, it is practical to use SNR of the full system for the comparison of the different configurations rather than the noise spectrum alone because the signal and the noise are amplified by the same factor.

### *1.2. Voltage and transimpedance amplification*

Four total options exist to amplify the tuning fork's signal. The input and the output of an amplifier can be either current or voltage, therefore producing four combinations: a voltage amplifier, a current amplifier, a transconductance amplifier, and a transimpedance amplifier.

In the case of mechanical excitation, the tuning fork response can be measured as a current or as a voltage.

First, a transimpedance configuration, which converts current into voltage, and, second, a high impedance configuration, which measures voltage directly. In either case, the small signal has to be amplified, and the output should be a voltage that is large enough to be processed by analog circuitry.

Therefore a voltage amplifier can be used if the tuning fork signal is measured as a voltage and a transimpedance amplifier can be used if the tuning fork signal is measured as a current.

The gain of a voltage amplifier is expressed as the ratio between input and output, whereas the gain of the transimpedance configuration is expressed in units of [V/A] or [Ω].

If the tuning fork is excited electronically, excitation can, in principle, be done by either voltage or current drive. In practice, current drive is hard to dimension for such high impedance as that of the tuning forks. Therefore, it is practical to excite it with a voltage [8] and detect the current with a transimpedance amplifier.

The background on the output signal caused by the driving input signal can be removed by cancelling it with a current that has equal amplitude but the opposite phase. This can be implemented by connecting a "dummy load" to the input terminal of the transimpedance amplifier, that is driven with the same frequency and amplitude signal but opposite phase. As this "dummy load" should have no resonance at the resonant frequency of the tuning fork, it is just a capacitor of roughly the same value as the capacitance of the real tuning fork. Precise cancellation of the two currents at the input of the amplifier is done by adjusting the amplitude ratio between the two driving counter-phase signals.

Electronic amplification is done by using operational amplifiers (OPAMPs), selected for minimal noise contribution [18–22]. In the case of the voltage amplifier (Fig. 9), the dominant noise source is the thermal noise due to the load resistor R1 at the input. As this resistor is placed parallel to the tuning fork, the thermal noise current, which scales with the square root of the resistor value, is added to the tuning fork signal current. For a low thermal noise current therefore the resistor value should be high compared to the tuning fork resistance (approx. 2 MΩ at 32 kHz). We use an OPAMP with a field-effect transistor input for its low input bias current and accompanying negligible current noise.

The capacitance of the tuning fork (2 pF), the input capacitance of the operational amplifier (8 pF) [23] and the stray capacitance of the wires at the input of the amplifier (1 pF) add up to a relatively large capacitance value (11 pF). The impedance of this total capacitance at the resonance frequency (close to 500 kΩ) is much lower than the load resistor value (10 MΩ) and the fork's voltage equals the current times the impedance of the total capacitance.

In the case of current sensing with a transimpedance amplifier (Fig. 8), the dominant noise source of the amplifier is the thermal noise due to the feedback resistor R4 (Fig. 8). Noise calculations are given in Appendix C. The thermal noise current adds to the signal current of the tuning fork, and this limits the SNR. R4 therefore needs to be as high as possible, where the limit is determined by the amplifier response speed where we need to maintain a bandwidth of least 34 kHz (R4 = 2.2 MΩ). R5 and R9 are added to boost the output voltage of the amplifier by a factor of 11. This does not affect the SNR as both the signal and the dominant noise get amplified by the same factor.

## 2. Methods

### *2.1. Setup*

To have a fair comparison of the SNR for the different methods of excitation and detection, we excited the tuning fork such that the oscillation amplitude is roughly the same in all cases, and we normalized the output signals to the oscillation amplitude (Fig. 5). To measure this amplitude, a test setup was constructed (Fig. 4). The detailed description of the setup can be found in Appendix B.

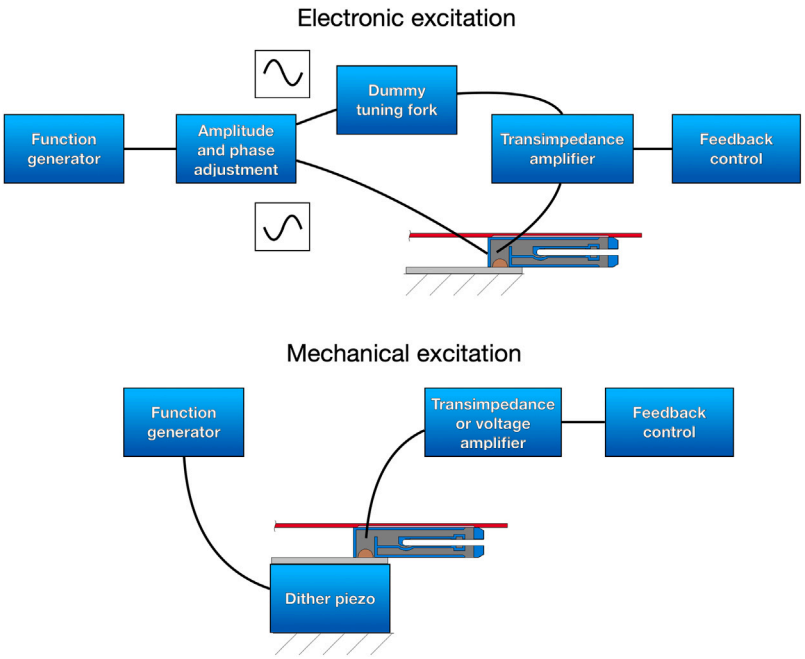


**Fig. 3.** Schematic representation of mechanical and electronic excitation.

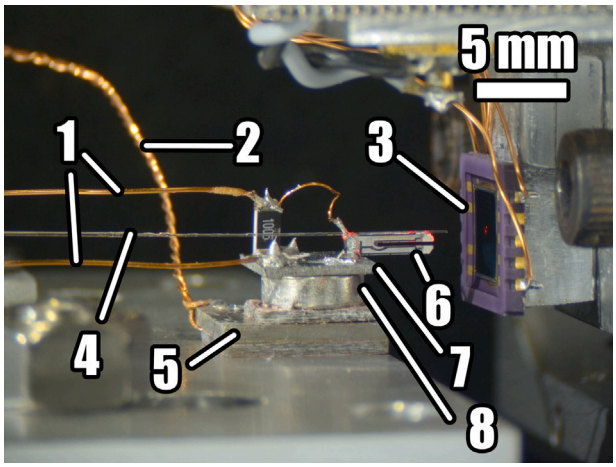


**Fig. 4.** The opto-mechanical part of the test setup. 1 - Tuning fork leads, soldered to a 10 MΩ resistor. 2 - Dither piezo leads. 3 - Segmented photodiode. 4 - Optical fiber. 5 - Dither piezo assembly. 6. - Tuning fork. 7 - Nickel base-plate. 8 - Neodymium magnet.

The signal from the function generator was either directly applied to the dither piezo for mechanical excitation, or served as the input signal for the electric excitation via the driving circuitry.

The sensitivity of the segmented photodiode was measured by adjusting its height and recording the voltage levels produced by the light spot coming out of the resting tuning fork, outfitted with an optical fiber.

The noise levels at the output of the amplifiers were measured without excitation of the tuning fork using a digital-to-analog converter (DAC).

### 2.2. Frequency response measurement

We characterized the frequency response of the tuning fork's excitation and detection system over a 5 kHz bandwidth surrounding the main resonance. We use a customized National Instruments LabVIEW Virtual Instrument (VI), consisting of two basic steps. First, we create a stimulus signal in frequency domain, in which all frequencies in the region of interest with desired frequency resolution are present. To avoid condensed power bursts, a randomized phase is assigned to each frequency. This stimulus is then converted to the time domain using an inverse Fourier transform, and applied. The response of the system is measured at one analog input of the DAC, while the stimulus is measured at another to avoid data acquisition artifacts. Both signals are converted into the frequency domain using the Fourier transform. The quotient of the response over the stimulus is calculated to determine the complex transfer function. This process is repeated (10 times) and the results are averaged. The amplitude and phase are shown in Fig. 6. It is worth to note that the behavior of the mechanically excited tuning fork contains unidentified mechanical resonances due to the complexity of the system, consisting of numerous mass–spring–damper elements. For the noise density spectrum measurement, we use a customized VI to produce the output spectrum in $V_{RMS}/\sqrt{Hz}$.

## 3. Results

Using the setup (Fig. 4), the fiber was connected to a laser and the vertical movement of the stage was calibrated to the output signal of the detector (Fig. 7). The tuning fork amplifiers then were connected in different configurations without moving the tuning fork assembly neither on its magnet nor relative to the detector so that the amplitude of the movement can be set at the same value for both excitation modes (43–45 nm at the resonance frequency). The tuning fork signal (before amplification) can now be calculated from the detector signal. The full overview of the results is shown in Appendix C, Table 1. In each configuration, the amplitude of the excitation signal was adjusted such that the tip moved 43–45 $nm_{RMS}$. The detection signal was normalized to the tuning fork's movement, and resulted in $8.61 \times 10^{-3}$ for the transimpedance amplifier and $18.7 \times 10^{-3}$ $V_{RMS}/nm$ for the voltage amplifier respectively.

The noise measurements must be performed to determine the SNR (Fig. 10). Zero voltage input for the voltage amplifier is accomplished by shorting the inputs. Zero current input for the transimpedance amplifier is achieved by leaving the inputs open.

Finally, the SNR was calculated based on the normalized signal. The transimpedance amplifier yielded $4.1{\times}10^3$ $\sqrt{Hz}/nm_{RMS}$ and the voltage amplifier $5.66 \times 10^3$ $\sqrt{Hz}/nm_{RMS}$.

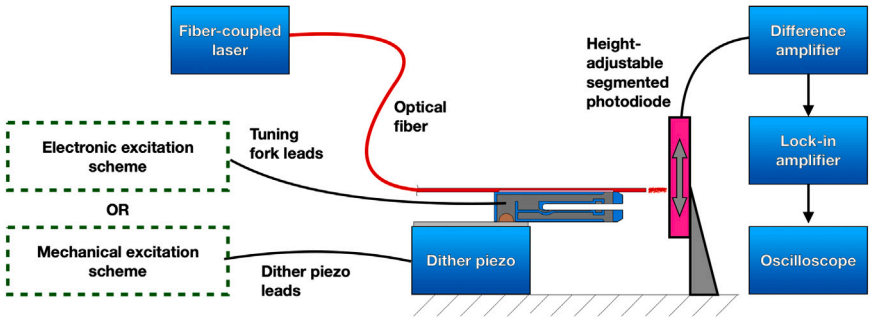


**Fig. 5.** Principle diagram of the experiment.

**Table 1**
Comparison table for the investigated configurations.

| Quantity and unit | Electronic excitation[a] | Mechanical excitation | |
|---|---|---|---|
| | TA | TA | VA |
| TF[b] signal [$mV_{RMS}$] | 379.7 | 379.8 | 812.9 |
| Amplified SP[c] signal on LIA [$mV_{RMS}$] | 10.9 | 10.7 | 10.2 |
| SP sensitivity [μm/V] | 4.16 | 4.12 | 4.26 |
| TF movement [$nm_{RMS}$] | 45.4 | 44.1 | 43.4 |
| TF signal, normalized [$V_{RMS}$/nm] | $8.36 \times 10^{-3}$ | $8.61 \times 10^{-3}$ | $18.7 \times 10^{-3}$ |
| Noise level [$V_{RMS}/\sqrt{Hz}$] | $2.1 \times 10^{-6}$ | $2.1 \times 10^{-6}$ | $3.3 \times 10^{-6}$ |
| SNR [$\sqrt{Hz}$] | $3.99 \times 10^{3}$ | $4.1 \times 10^{3}$ | $5.66 \times 10^{3}$ |

[a]Reference values.
[b]Tuning fork.
[c]Segmented photodiode.

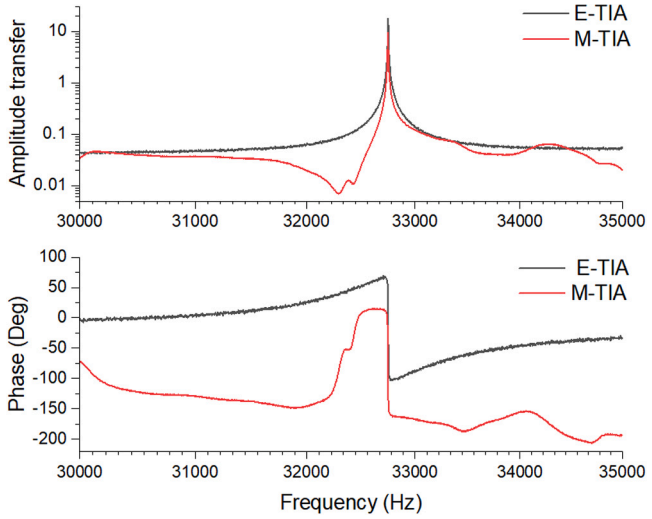


**Fig. 6.** Amplitude (top) and phase (bottom) transfer measurements of a bare tuning fork using mechanical (M-) and electronic (E-) excitation, with amplification by the transimpedance amplifier (TIA).

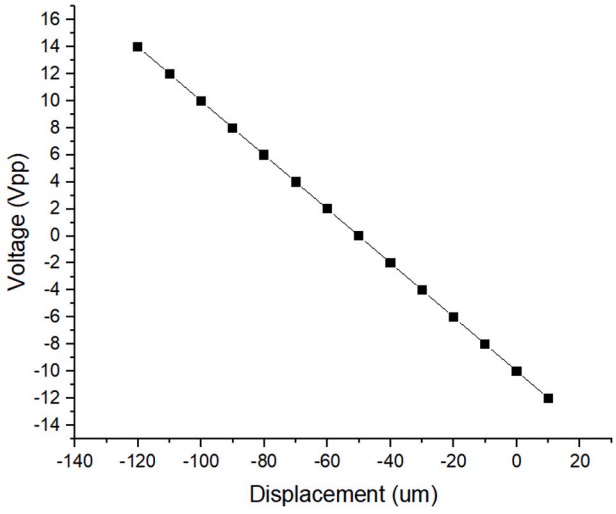


**Fig. 7.** Displacement-voltage curve for calibration of the segmented photoelectric cell. The vertical axis corresponds to the difference between signals of the optical segments.

## 4. Discussion

### 4.1. Signal-to-noise ratio

The noise spectra are shown in Fig. 10. As the current detection with both the mechanical and the electronic excitation uses the transimpedance amplifier, these noise spectra are equal. Due to capacitances and a 60 kHz anti-aliasing filter, this noise rolls off at 60 kHz, well above the frequency of interest.

It is evident that the particular method of excitation of vibration does not significantly shift the resonant frequency of the tuning fork assembly, but the choice of the amplification circuit does affect the shape of the amplitude response, and, hence, the Q-factor can vary. The electronic excitation has a clear advantage over the mechanical due to the absence of local minima and maxima in the amplitude–frequency characteristic (Fig. 6). The fact that the electronic excitation is less sensitive to mechanical instability is further supported by the measurement of the amplitude transfer characteristics of a complete measurement head unit in which both methods of actuation are simultaneously implemented (Fig. 11). Using the (0–10 μm) of the height control piezo as the independent variable we show the change in amplitude transfer and phase characteristic of the tuning fork assembly. While cross-talk between the piezo position and the oscillation amplitude is obvious for the mechanical excitation mode, hardly any difference presents itself in the case of electronic excitation (Fig. 12).

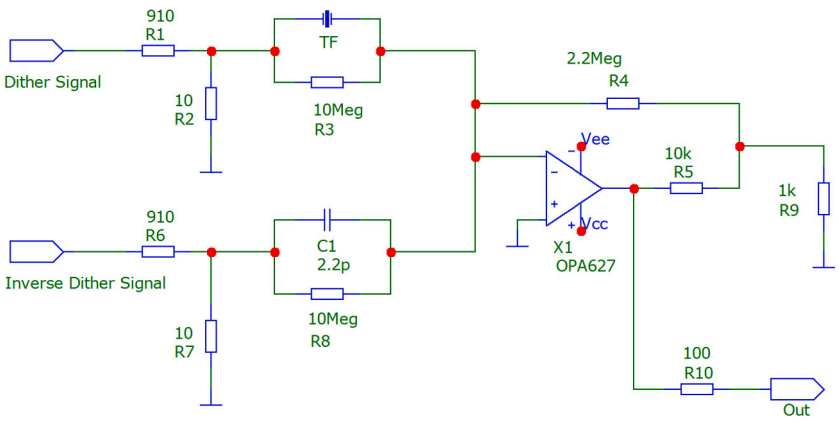


**Fig. 8.** Diagram of the OPA627-based transimpedance amplifier with electronic excitation.

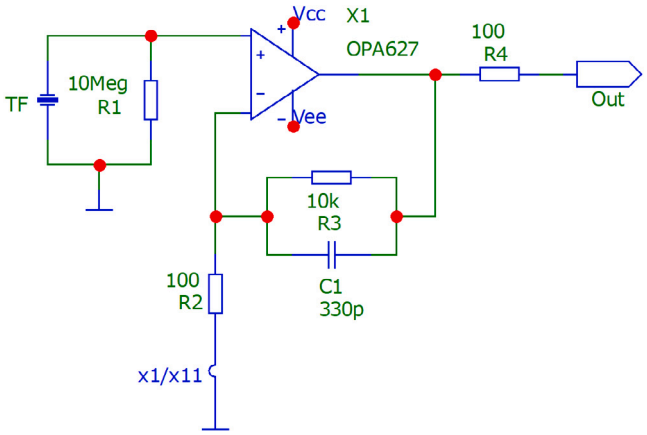


**Fig. 9.** Diagram of the OPA627-based voltage amplifier.

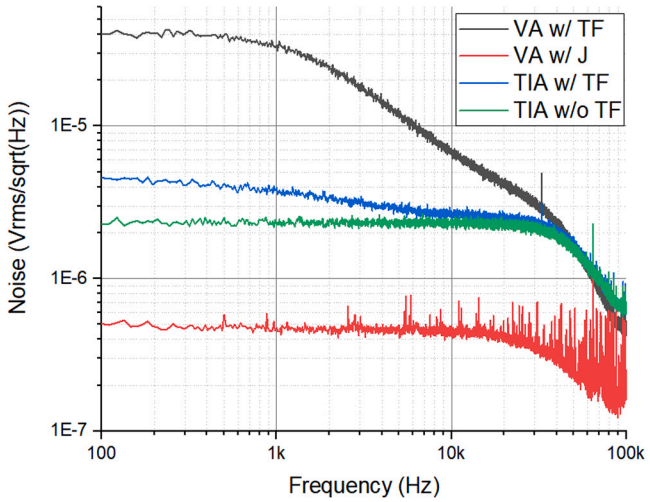


**Fig. 10.** Voltage noise density frequency-characteristics for the transimpedance (TIA) and voltage (VA) amplifiers with and without the tuning fork (TF) attached, or with a jumper (J) shorting the input contacts.

The cleanliness of the amplitude characteristic and comparable noise performance results in overall preferability of the electronic excitation.

### 4.2. Outlook

From the operation of the voltage amplifier we can conclude that the main noise contribution comes from the resistor R1 (Fig. 9). The noise level could be further reduced by choosing a higher value for it, although the input capacitance is limiting the signal level. For high gain and high offset currents, the output of the voltage amplifier can become saturated. This could be avoided by adding a capacitor in series with R2 to have the unity gain at DC [24,25], while keeping the gain of 101× at the frequencies of interest.

The dominant noise contribution in the transimpedance amplifier circuit comes from the feedback resistor R4 (Fig. 8), and the SNR could be improved by replacing it with a 2.2 pF capacitor, such that the impedance at 32 kHz would be approximately the same. This would create a charge amplifier, where it remains to be seen whether this is feasible. To provide a DC path from the output to the input, a 1 GΩ resistor can be connected in parallel. This resistor exhibits less thermal noise current than that of the 2.2 MΩ resistor.

## 5. Conclusion

Characterization of different excitation methods and tuning fork signal amplifiers was done by comparing the vibration transfer from the excitation source to the signal output at equal tuning fork oscillation amplitudes. Measurements were performed on two different actuation modes and it was found that for a given amplifier, the SNR does not depend on the method of actuation, as long as the same amplitude of vibration is maintained. The measured noise values match the theoretical values and yield comparable SNR for the different excitation methods. The presence of the tuning fork does not significantly impact the noise level of the amplifiers. Electronic excitation of the tuning fork has an advantage over mechanical excitation as it is less impacted by artifacts caused by mechanical instability of the system.

## Declaration of competing interest

The authors declare that they have no known competing financial interests or personal relationships that could have appeared to influence the work reported in this paper.

## Data availability

Data will be made available on request.

## Acknowledgments

The authors would like to thank F. B. Segerink, Optical Sciences Group, Department of Science and Technology, University of Twente.

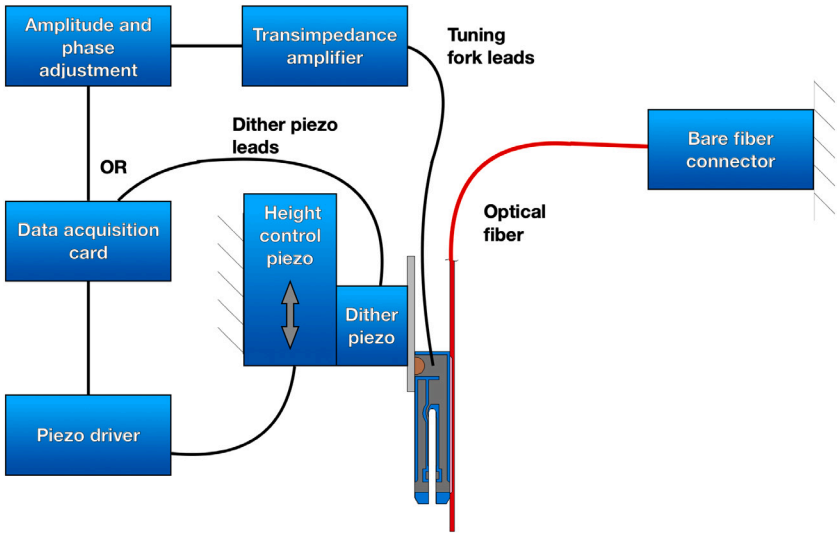


**Fig. 11.** Schematic representation of the part of the microscope scanning head with the fiber attached to the tuning fork on one end, and to the bare fiber connector on the other.

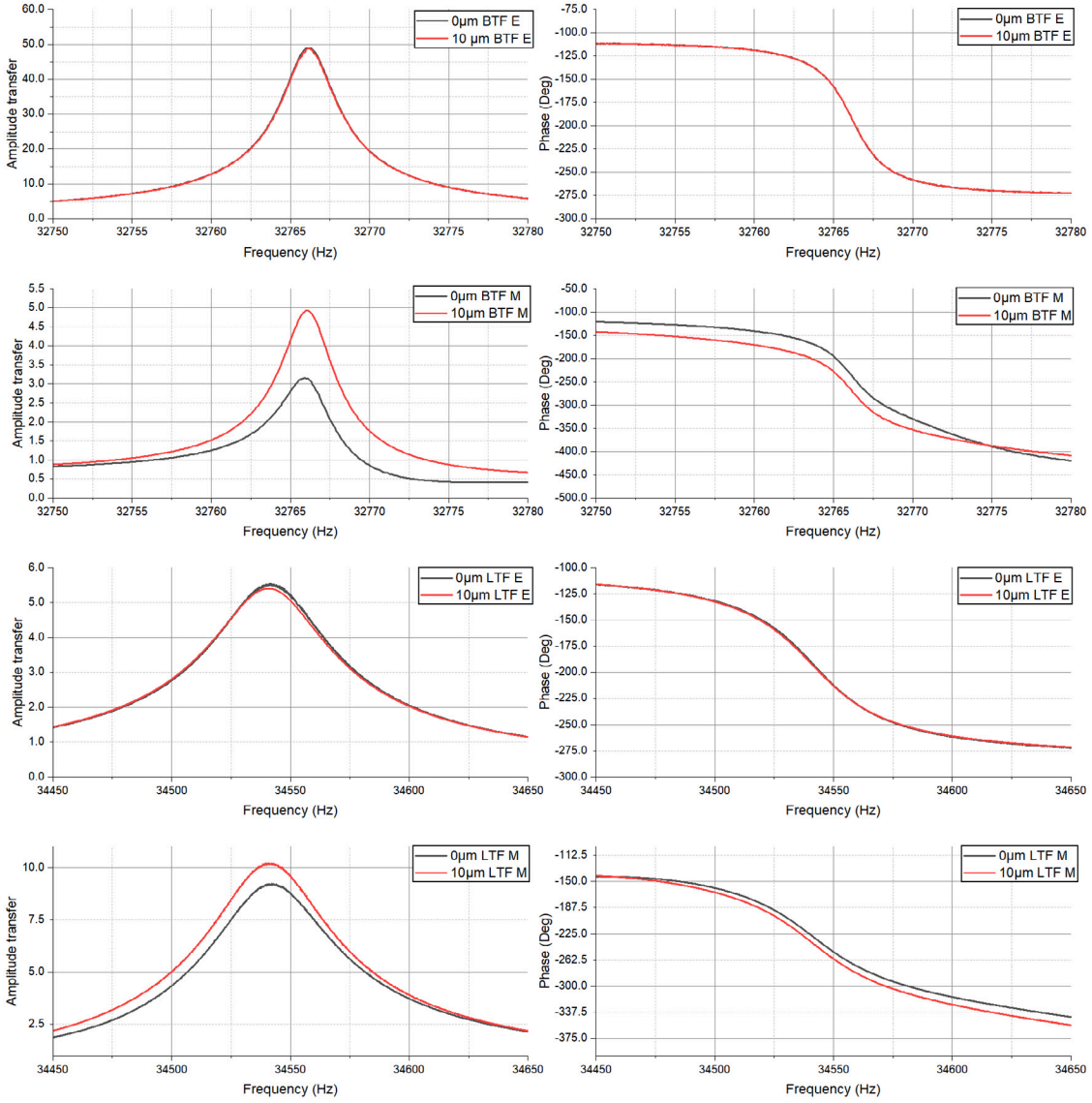


**Fig. 12.** Amplitude transfer and phase characteristic of the tuning fork, excited either mechanically (M) or electronically (E), loaded with fiber (LTF) or bare (BTF) supported by either relaxed or extended (10 µm) height control piezo-actuator, with signal amplified by transimpedance amplifier. Note how the mechanical excitation significantly changes the amplitude transfer and phase characteristic nearby the resonance frequency.

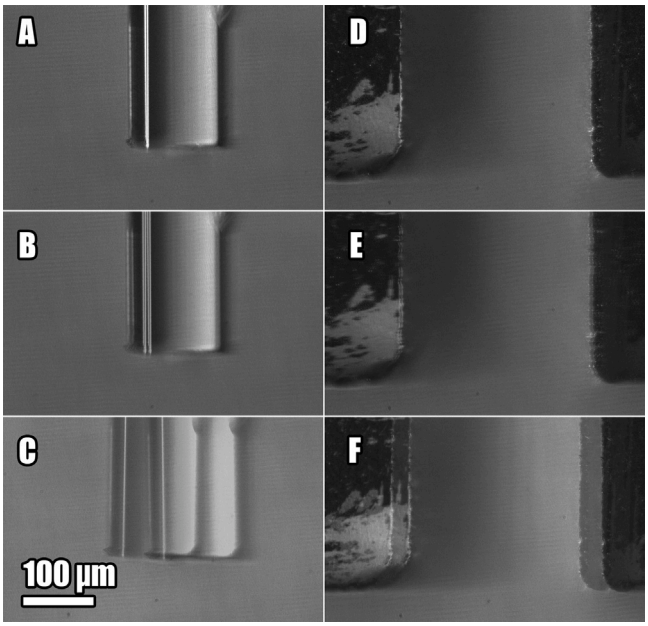


**Fig. 13.** Optical microscope image of movement of the tip of the fiber (A-C) and the prongs of the tuning fork (D-F) excited mechanically (B, E) and electronically (C, F). B, C, E, F were obtained by superimposing frames of a video recording.

## Appendix A. Movement of tuning fork probes

As we have noted earlier, the movement of the tuning fork prongs and, hence the tip of the optical fiber, have the same character regardless of the type of excitation. To verify this experimentally by direct observation, an additional experiment was set up. The tuning fork, outfitted with a fiber, was placed on a dither piezo directly under the optical microscope such that both prongs are in the focus plane, and illuminated from the side with a white-light laser. Both the excitation and the triggering signal for the illumination were produced by a synchronized two-channel function generator. The excitation signal was set up at the resonant frequency of the loaded tuning fork and further amplified by a high-voltage amplifier up to 200 $V_{PP}$, and the frequency of the trigger signal offset by a few Hz to produce movement slow enough to be resolved by a conventional camera. The driving voltage was then directed either to the dither piezo or the tuning fork's leads without moving the observed specimen in relation to the microscope lens.

A series of video recordings were then taken (available upon request). Observation of the superimposed still frames (Fig. 13) confirms the expected outcome and FEM modeling. In both cases the prongs moved in the symmetric mode, and the amplitude of the tip of the fiber exceeded that of the tip of the prongs. The common-mode movement of the prongs or the base of the tuning fork was not observed. The maximum expected amplitude of the dither piezo displacement is less than 100 $nm_{PP}$, based on the sensitivity and applied voltage. While the efficiency of the types of excitation is, obviously, very different, it remains outside of the scope of the current work.

## Appendix B. Experimental setup

The measurements were carried out on a Newport [26] technical series sealed hole laboratory table top (244 × 122 × 20 cm), isolated by 4 NRC pneumatic isolation mounts, type XL-G. A dither piezo (Philips PXE 5, 0.5 nm/V) is secured to the table. On top of it a magnet is glued that holds a laser-cut nickel plate (7 × 7 × 0.5 mm) on which the quartz tuning fork (ABRACON AB38T-32.768 KHZ) is soldered. This composition assures that the vibration transfer from the dither piezo to the tuning fork and efficiency are mainly in the vertical direction. The fiber (Thorlabs SM800-5.6-125, length ca. 30 cm), is glued to the top tuning fork's prong with two-component epoxy and is illuminated with a solid-state laser (Thorlabs LPS-635-fc, operating at 1.0 mW). A segmented photoelectric cell (PEC, Hamamatsu S5980) is placed facing the fiber tip on a micrometric translation stage (Spindler & Hoyer Lineartisch MR80-25 Typ: C01-338070). A function generator (Stanford Research Systems DS335) provided a stable, low-noise excitation signal. A lock-in amplifier (Stanford Research Systems SR530) was used to pick up the output of the PEC at the resonant frequency. The tuning fork output signal after the amplifier was measured using the lock-in amplifier and an oscilloscope (Tektronix TDS2014). An 11× attenuator was used to scale the voltage signal down to an acceptable level for the lock-in amplifier to prevent saturation of the input signal, and a 60 kHz low-pass filter was used to prevent aliasing. The noise levels were measured using DAC (National Instruments PCI-6259 with BNC-2110 connector block).

## Appendix C. Noise analysis

To conduct investigation into the dominant noise sources, a SPICE simulation of noise equivalent circuits was conducted and compared against the measured characteristics (Fig. 14). The resistor R4 (Fig. 8) has a value of 2.2 MΩ, and hence the thermal noise voltage equals 189 $nV/\sqrt{Hz}$. Due to R5 and R9, the thermal noise voltage will be amplified by a factor of 11, so that a noise density of 2.1 $\mu V/\sqrt{Hz}$ is expected and observed at low frequencies.

The noise spectrum of the voltage amplifier is dominated by the thermal noise of the 10 MΩ load resistor R1 for the low frequencies (Fig. 9) of $4.0\times10^2$ $nV/\sqrt{Hz}$. The voltage amplifier gain is 101× in this frequency region, so that the expected and observed noise density at the output of the voltage amplifier is 41 $\mu V/\sqrt{Hz}$. The roll-off at 1.5 kHz

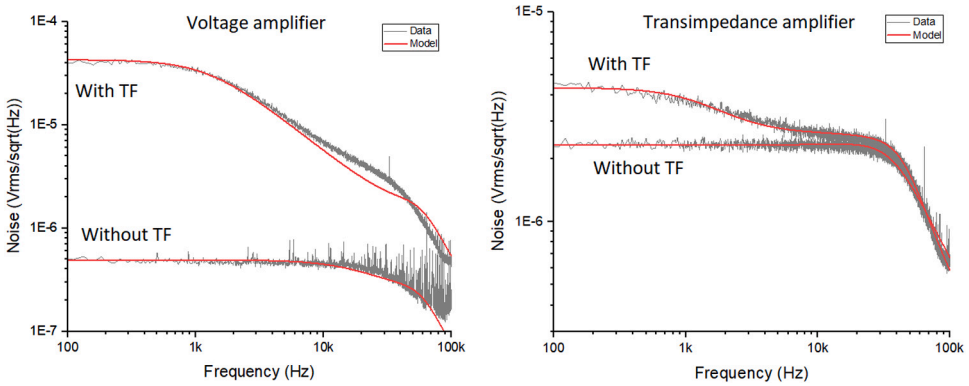


**Fig. 14.** Comparison of SPICE model to the measured noise characteristics.

can be traced to the capacitance at the input of the voltage amplifier in parallel to the load resistor of 10 MΩ. This capacitance is the sum of the tuning fork capacitance (2 pFt, measured by balancing out the background signal in electronic excitation scheme with a capacitor), the input capacitance of the OPA627 (8 pF, taken from the datasheet), and the capacitance of the wiring and the circuit board tracks (1 pF, estimated from Fig. 10, −3 dB cut-off frequency of VA w/TW). The roll-off frequency is given by, $f = 1/2 \times \pi RC$, so that the total capacitance must equal 11 pF. Due to this capacitance, the thermal noise of the load resistor is attenuated down to 3.3 $\mu V/\sqrt{Hz}$ at 32 kHz.

The signal current for mechanical excitation can be calculated from the output signal of the transimpedance amplifier and yields 8.36 $mV_{RMS}$ per nm of tuning fork's movement. Based on the 2.2 MΩ transimpedance gain and a built-in voltage gain of 11×, the tuning fork signal current can be estimated to be 345 $pA_{RMS}$ per nm tuning fork movement. In case of the voltage amplifier, this signal current is flowing through a load impedance, which is dominated by the capacitance that was shown to be 11 pF. When we multiply the signal current with the impedance of this capacitor at frequency of interest, the signal voltage at the input of the voltage amplifier can be estimated to be 0.156 $mV_{RMS}$ per nm. The voltage amplifier has the gain of 101×, so the output signal is 15.8 $mV_{RMS}$ per nm of the tuning fork's movement in this case. The measured signal of 18.7 $mV_{RMS}$ is in good agreement with this.

## References


[1] F.J. Giessibl, High-speed force sensor for force microscopy and profilometry utilizing a quartz tuning fork, Appl. Phys. Lett. 73 (1998) 3956–3958.

[2] F.F. Froehlich, T.D. Milster, Mechanical resonance behavior of near-field optical microscope probes, Appl. Phys. Lett. 70 (1997) 1500–1502.

[3] G.M. King, G. Nunes, Attractive-mode force microscope for investigations of biomolecules under ambient conditions, Rev. Sci. Instrum. 72 (2001) 4261–4265.

[4] G.M. King, J.S. Lamb, G. Nunes, Quartz tuning forks as sensors for attractive-mode force microscopy under ambient conditions, Appl. Phys. Lett. 79 (2001) 1712–1714.

[5] W.H.J. Rensen, N.F. van Hulst, A.G.T. Ruiter, P.E. West, Atomic steps with tuning-fork-based noncontact atomic force microscopy, Appl. Phys. Lett. 75 (1999) 1640–1642.

[6] H. Edwards, L. Taylor, W. Duncan, A.J. Melmed, Fast, high-resolution atomic force microscopy using a quartz tuning fork as actuator and sensor, J. Appl. Phys. 82 (1997) 980–984.

[7] C. Durkan, I.V. Shvets, Study of shear force as a distance regulation mechanism for scanning near-field optical microscopy, J. Appl. Phys. 79 (1996) 1219–1223.

[8] K. Karrai, R.D. Grober, Piezoelectric tip-sample distance control for near field optical microscopes, Appl. Phys. Lett. 66 (1995) 1842.

[9] R. Toledo-Crow, P.C. Yang, Y. Chen, M. Vaez-Iravani, Near-field differential scanning optical microscope with atomic force regulation, Appl. Phys. Lett. 60 (1992) 2957–2959.

[10] E. Betzig, P.L. Finn, J.S. Weiner, Combined shear force and near-field scanning optical microscopy, Appl. Phys. Lett. 60 (1992) 2484–2486.

[11] L. Novotny, B. Hecht, Principles of Nano-Optics, vol. 9781107005, Cambridge University Press, Cambridge, 2009, pp. 1–564.

[12] C.L. Jahncke, O. Brandt, K.E. Fellows, H.D. Hallen, Choosing a preamplifier for tuning fork signal detection in scanning force microscopy, Rev. Sci. Instrum. 75 (8) (2004) 2759–2761.

[13] K.B. Shelimov, D.N. Davydov, M. Moskovits, Dynamics of a piezoelectric tuning fork/optical fiber assembly in a near-field scanning optical microscope, Rev. Sci. Instrum. 71 (2000) 437–443.

[14] B. Kim, J. Jahng, R.M. Khan, S. Park, E.O. Potma, Eigenmodes of a quartz tuning fork and their application to photoinduced force microscopy, Phys. Rev. B 95 (7) (2017) 075440, arXiv:1612.07253.

[15] A.G. Ruiter, K.O.V.D. Werf, J.A. Veerman, M.F. Garcia-Parajo, W.H. Rensen, N.F.V. Hulst, Tuning fork shear-force feedback, Ultramicroscopy 71 (1998) 149–157.

[16] W.H.J. Rensen, Tuning fork tunes: exploring new scanning probe applications, 2002.

[17] S. Chuang, Quartz tuning fork crystal using overtone flexure modes, in: Thirty Fifth Annual Frequency Control Symposium, IEEE, 2008, pp. 130–143.

[18] J. Dostal, Operational Amplifiers, second ed., Butterworth-Heinemann, 1993.

[19] J. Ragazzini, R. Randall, F. Russell, Analysis of problems in dynamics by electronic circuits, Proc. IRE 35 (1947) 444–452.

[20] R. Nave, Practical benefits: Negative Feedback. http://hyperphysics.phy-astr.gsu.edu/hbase/Electronic/feedn.html. (Accessed: 7 February 2023).

[21] B. Carter, R. Mancini, in: B. Carter, R.B.T.O.A. for Everyone (Fifth Edition) Mancini (Eds.), Feedback and Stability Theory, Elsevier, 2018, pp. 59–75,

[22] B. Carter, R. Mancini, Op Amps for Everyone, Elsevier, 2009.

[23] Texas Instruments: OPA627 and OPA637 Precision High-Speed Difet Operational Amplifiers. https://www.ti.com/lit/ds/symlink/opa627.pdf. (Accessed: 7 February 2023).

[24] P. Horowitz, W. Hill, The Art of Electronics, third ed., Cambridge University Press, USA, 2015.

[25] P. Horowitz, W. Hill, The Art of Electronics: The X Chapters, Cambridge University Press, 2020.

[26] Newport Corporation website. http://www.newport.com (Accessed: 7 February 2023).